SCIENTIFIC REPORTS

OPEN

SUBJECT AREAS:

SENSORS AND BIOSENSORS

OPTICAL MATERIALS

FLUORESCENCE SPECTROMETRY

SELF-ASSEMBLY

Received
3 May 2013

Accepted
25 July 2013

Published
4 September 2013

Correspondence and requests for materials should be addressed to M.M. (manuela.melucci@isof.cnr.it) or M.C. (m.cavallini@bo.ismn.cnr.it)

A time-temperature integrator based on fluorescent and polymorphic compounds

Denis Gentili[1], Margherita Durso[2], Cristian Bettini[3], Ilse Manet[2], Massimo Gazzano[1], Raffaella Capelli[1,4], Michele Muccini[1,4], Manuela Melucci[2] & Massimiliano Cavallini[1,5]

[1]Consiglio Nazionale delle Ricerche-Istituto per lo studio dei Materiali Nanostrutturati (CNR- ISMN), via P. Gobetti 101, 40129 Bologna, Italy, [2]Consiglio Nazionale delle Ricerche -Istituto per la Sintesi Organica e la Fotoreattività, (CNR-ISOF), via P. Gobetti 101, 40129 Bologna, Italy, [3]Laboratorio MIST E-R, via P. Gobetti 101, 40129 Bologna, Italy, [4]ETC s.r.l., via P. Gobetti 101, 40129 Bologna, Italy, [5]SCRIBA Nanotecnologie s.r.l. Via P. Gobetti 52/3, 40129 Bologna, Italy.

Despite the variety of functional properties of molecular materials, which make them of interest for a number of technologies, their tendency to form inhomogeneous aggregates in thin films and to self-organize in polymorphs are considered drawbacks for practical applications. Here, we report on the use of polymorphic molecular fluorescent thin films as time temperature integrators, a class of devices that monitor the thermal history of a product. The device is fabricated by patterning the fluorescent model compound thieno(bis)imide-oligothiophene. The fluorescence colour of the pattern changes as a consequence of an irreversible phase variation driven by temperature, and reveals the temperature at which the pattern was exposed. The experimental results are quantitatively analysed in the range 20–200°C and interpreted considering a polymorph recrystallization in the thin film. Noteworthy, the reported method is of general validity and can be extended to every compound featuring irreversible temperature-dependent change of fluorescence.

In recent years a number of organic and hybrids new materials combining different functionalities have been synthesized. This constant interest in multifunctional materials (MMs) is due to the large spectrum of fundamental properties that find application in many technological fields. For instance, limiting the application to solid-state, MMs have been exploited in: electronics, both as active[1] and passive[2,3] elements, opto-electronics[4,5], non-linear optics[6], photonics[7], photovoltaics[8], spintronics[9], magnetism[10], permanent/erasable[11,12] memories and sensing[13]. In the last two decades, most of these applications have been oriented toward nanotechnology due to the possibility of combining the intrinsic properties of MMs related to their chemical structure, with the new properties arising from their assembly and spatial distribution at the micro- and nanoscale[14,15].

Among various MMs, thiophene-based compounds[16–19] play a key role in the materials scenario due to their chemical versatility, functional properties, extraordinary self-organizing properties at multiple length scales[20] and excellent processability[21,22].

Despite the variety of available functional properties, to date, efforts in MMs design have been mainly addressed toward the optimization of the charge transport and light emitting properties, in view of their use in thin film organic devices such as organic field effect transistors (OFETs)[23–25], organic light emitting diodes (OLEDs)[26] and organic light emitting transistors (OLETs)[4,5]. However, many MMs exhibit polymorphism and/or a dependence of photophysical properties from the temperature; such features were considered detrimental for established applications such as OFETs, OLEDs, OLETs, etc., therefore a lot of these materials were considered, until now, of limited value and with no application potential.

In our work we demonstrate that based on this broadly occurring effect, and using proper processing (*viz.* controlling the partial pressure of the solvent) and patterning procedures, an important application can be targeted, which opens new perspectives for practical applications of a large variety of MMs.

In particular we report on the morphological/photophysical correlation with the temperature exposure of the MMs thin deposit that can be exploited to fabricate a real time-temperature integrator (TTI) device, i.e. a device capable to record the thermal history of the system.

The development of TTIs is of high interest for the traceability of perishable products, whose temperature must be maintained throughout a shipping or life cycle (e.g. food, pharms, drugs, but also some electronic devices). The most reliable TTIs are based on electronic sensors such as Radio Frequency IDentification (RFID) tags, whose cost and complexity limit their large-scale penetration in the market. Indeed, our device is printable and can be

manufactured as a label at extremely low cost. Further approaches to TTIs are based on irreversible colour changes exploiting: i) diffusion of a dye across a device[27], ii) enzymatic hydrolysis of a lipid substrate[28]; iii) patterned discotic liquid crystals[29]; iv) solid-state polymerization; v) dewetting of polymeric thin films[30]. These devices are very efficient for a single threshold temperature measurement; however, their complexity and fabrication hurdles dramatically increase when it is required to monitor a spectrum of temperatures. Indeed, in this case it becomes necessary to introduce different materials/components, each one sensitive to a specific critical temperature, in an independent device.

Here, taking advantage of the temperature-dependent fluorescence of the model compound thieno(bis)imide end-functionalized terthiophene **1**[4,5], (Fig. 1a), we introduce a new simple approach to fabricate TTIs based on the use of polymorphic crystalline aggregates controlling the spatial distribution of polymorphs. We demonstrate that a logic pattern (i.e. a pattern able to store information as a miniaturized data matrix code) of compound **1** functions as a TTI in wide temperature range. We choose compound **1** as model compound because it is currently subject of intense research in our group and we gained deep knowledge of its fundamental properties. In particular, **1** is highly processable in solution and it exhibits an ideal behaviour for TTI applications with a continuous variation of the fluorescence upon thermal treatment (other materials may show a phase transition at a defined threshold temperature) that allowed us to advantageously exploit the polymorphism. However, our approach is general and can be used for many other systems, including other polythiophene, polymers and hybrid systems.

Results

Thin films. Thin films of **1**, whose synthesis is described elsewhere[31], were grown by drop casting. Despite its short size, when deposited on a surface, **1** exhibits an extraordinary tendency to form crystals, whose size and shape depend on the experimental procedure and the solvent employed.

In order to compare the effects of the shrinking rate, which plays a key role on the thin film properties, we used chloroform and toluene that have comparable solvent properties but very different vapour tensions (Chloroform 21300 Pa at 20°C; Toluene 2900 Pa at 20°C). Thin deposits were investigated by means of polarized optical microscopy (POM), atomic force microscopy (AFM), fluorescence microscopy (FM), X-ray diffraction (XRD) and laser scanning confocal microscopy (LSCM).

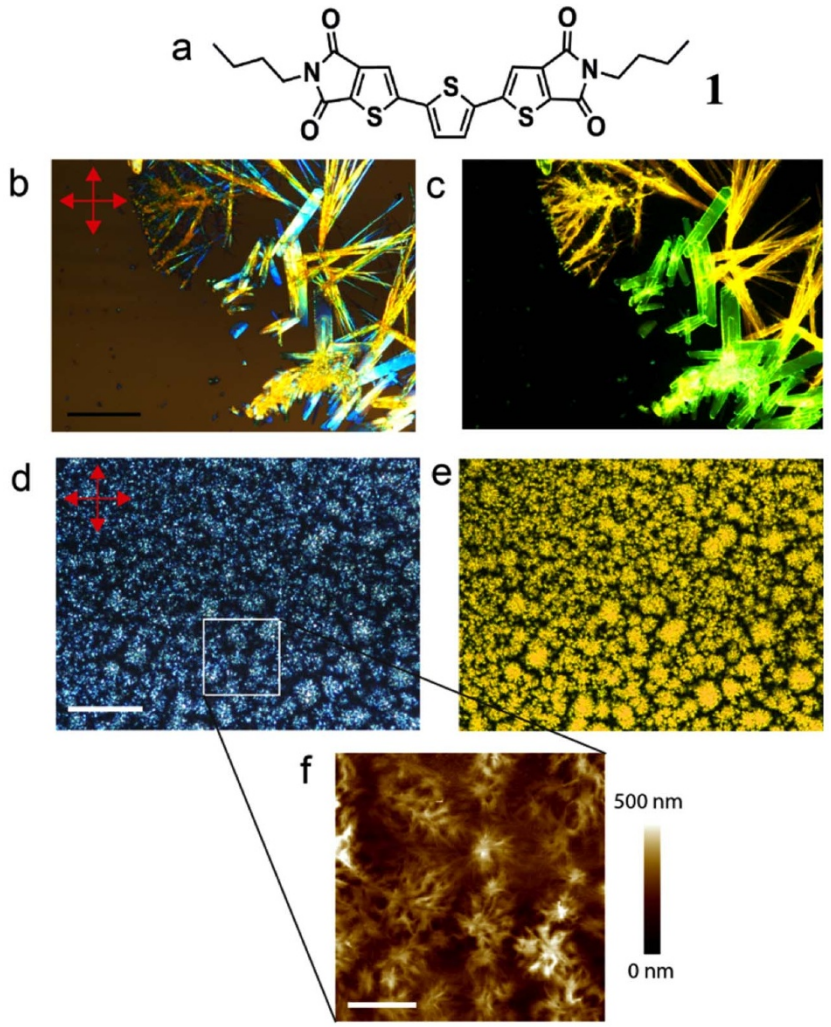

Figure 1 | Thin deposits observed by optical and fluorescence microscopy. (a) Chemical structure of **1**. (b) Optical micrograph of a drop cast thin deposit of **1** (toluene 1 g/L on Si/SiO_2 wafer) recorded with cross polarizers oriented as indicated by the red arrows; the bar scale is 20 μm. (c) Corresponding fluorescence microscopy image. (d) Optical micrograph of a drop cast thin deposit of **1** (chloroform 1 g/L on Si/SiO_2 wafer in air). Cross polarizers were oriented as indicated by the red arrows and (e) corresponding fluorescence microscopy image; the bar scale is 15 μm. f) AFM morphology of the same film; the bar scale is 8 μm.

When deposited from toluene in air, **1** shows two types of crystal morphologies, viz. fiber-like (fiber) and platelet-like (platelet) crystals (Fig. 1b). Fibers appear as long crystallites (>1 mm) randomly distributed on the surface. Their width ranges from 10 μm to 100 μm resulting in an aspect ratio (length/width) between 1 : 5 and > 1 : 10. Differently, platelets show the typical regular shape of crystals with well-defined angles, with size between 1 μm and > 500 μm and with an aspect ratio ranging between 1 : 2 and 1 : 5. Usually, platelets are about 75% (estimated value) of the total. No continuous film was observed in between the crystals by AFM or LSCM analysis.

Both platelets and fibers exhibit birefringence under POM (Fig. 1b). In particular, the platelets show the typical behaviour of optically anisotropic materials with extinction at precise orientations (i.e. when the long axis of the crystal is oriented 45° with respect to the polarisers). The occurrence of light extinction at the same orientations in each crystal suggests that they are either single crystals or formed by domains oriented in the same direction. The fibers exhibit a strong birefringence, but they appear multicoloured and do not extinguish at any directions (only a slight decrease of the intensity was occasionally observed), indicating their polycrystalline nature. Noticeably, a strong fluorescence was observed from both fibers - yellow colour- and platelets - green colour (Fig. 1c).

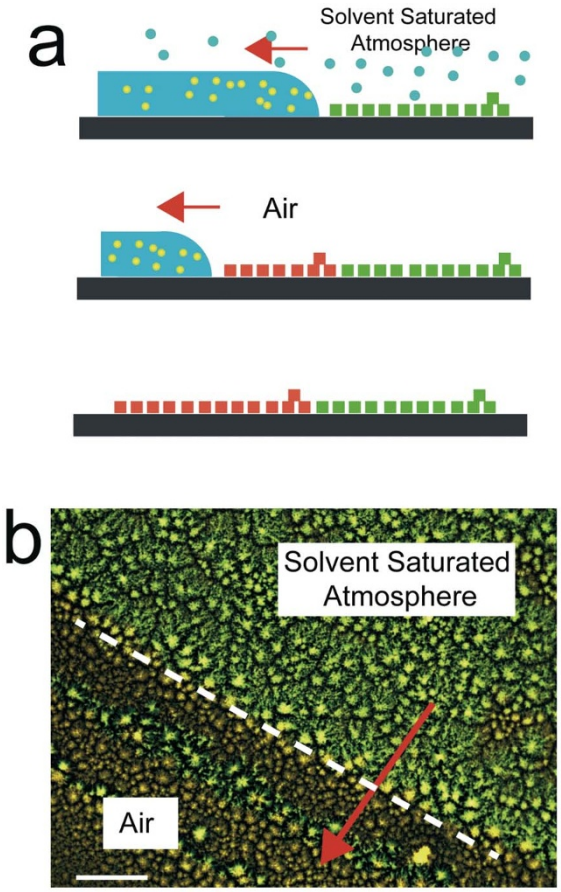

Figure 2 | Effect of the shrinking rate on polymorphs formation. (a) Scheme of the experiment: a drop of solution shrinks in atmosphere of saturated solvent vapour, as the atmosphere is suddenly removed the shrinking rate increases. (b) Fluorescence microscopy images of thin film of **1** recorded during the shrinking of 20 μl of 1 g/L chloroform solution. The front of shrinking solvent recedes in the direction indicated by the red arrow. The saturated atmosphere was removed in correspondence of the dotted line where the fluorescence changes from green to yellow; the bar scale is 15 μm.

When **1** is deposited from chloroform solution in a vapour-saturated environment, which in our experimental conditions shrank more than 2 times faster than toluene in air, we still observed a significant quantity of platelets (~60%, estimated value) but with a mean size reduced to few micrometres. If the same solution is deposited in air, where the shrinking rate is further increased (about 10 time faster than toluene in our experimental conditions), the percentage of fibers increases to more than 95% of the total (Fig. 1f).

This behaviour suggests that fibers are kinetically favoured, while platelets are the most thermodynamically stable phase. In order to confirm this hypothesis we performed an experiment changing the shrinking rate during the deposition. 50 μl of chloroform solution were deposited in a saturated atmosphere on a silicon substrate, and then the saturated atmosphere was removed during the shrinking (i.e. when the solid film started to form, figure 2a). Therefore, part of the film was obtained under slow shrinking rate, while another part was formed at higher shrinking rate. As clearly emerges from the florescence image shown in figure 2b, we observed a change of fluorescence colour when the saturated atmosphere is removed. Furthermore, the thermodynamic stability of platelets is confirmed by recrystallization via melting and quenching processes that transform fibers into platelets (see supplementary information).

To gain an insight on the morphology-dependent fluorescence of the thin deposits of **1**, X-Ray diffraction (XRD) and Laser Scanning Confocal Microscopy (LSCM) were performed on samples containing a majority (>90%) of fibers or a majority (>90%) of platelets.

Low-angle XRD analysis revealed two different diffraction profiles with the main peak at an angle corresponding to interplanar distances of 2.2 nm (green curve, Fig. 3a) and 2.1 nm (red curve, Fig. 3a) for films of **1** containing a majority of platelets or fibers, respectively. As a confirmation, in a film showing both types of crystals both sequences of reflexes can be found (blue curve, Fig. 3a).

Figure 4a shows an LSCM image of platelets and fibres of **1** and the corresponding confocal PL spectra (Fig. 4b) recorded in the regions marked by circles in figure 4a. PL spectra confirm the FM image showing an emission centred at 542 nm for the platelets and at 585 nm for fibril-like crystals. Time-resolved fluorescence lifetime imaging measured in the range 500–540 nm and 565–605 nm ranges confirmed that the self-assembled fluorophore experienced two locally different environments. In fact analysing the fluorescence decay at 585 nm with a bi-exponential function the fibres have a dominating lifetime of 1.0 ± 0.2 ns, while for the green crystals a triexponentail fit is required; the lifetime of 0.45 ± 0.1 ns prevails and the 1.0 ns lifetime contributes to a less extent (Fig. 4c,d).

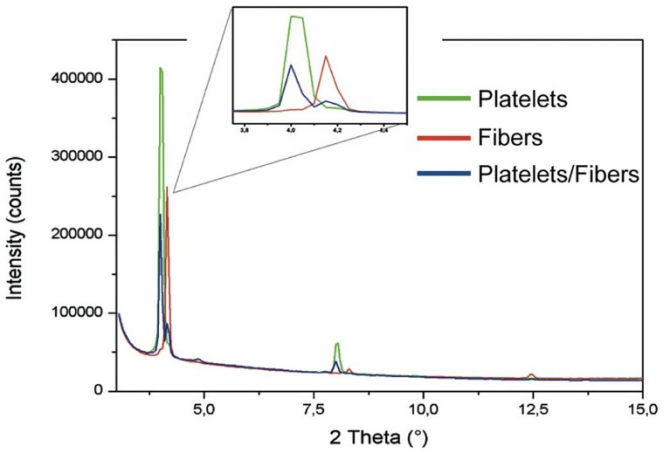

Figure 3 | X-Ray diffraction. Diffraction patterns of three different films on a Si/SiO_2 substrate having a majority of platelets (green curve), fibers (red curve) and a mixture of platelets and fibers (blue curve).

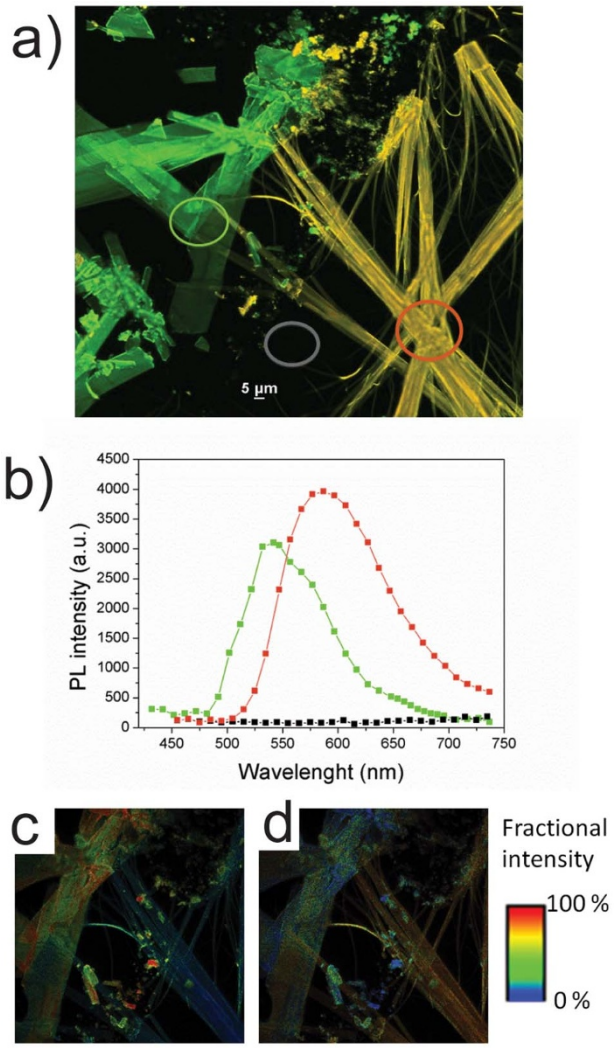

Figure 4 | Laser scanning confocal fluorescence microscopy characterization of crystals. (a) Confocal fluorescence microscopy image of crystals and fibers of **1**, the image is a merge of fluorescence collected with two PMT with bandpass filters 525/50 nm and 595/50 nm. b) Confocal PL spectra measured for the background region (black), the platelets (green) and the fibers (yellow), indicated in 4a by the circles. c, d) fluorescence lifetime images of the central part of (b). Each pixel represents the fractional intensity of the 0.45 ns (c) and 1.0 ns (d) lifetimes, respectively. The colour scale ranges from 0% (blue) to 100% (red).

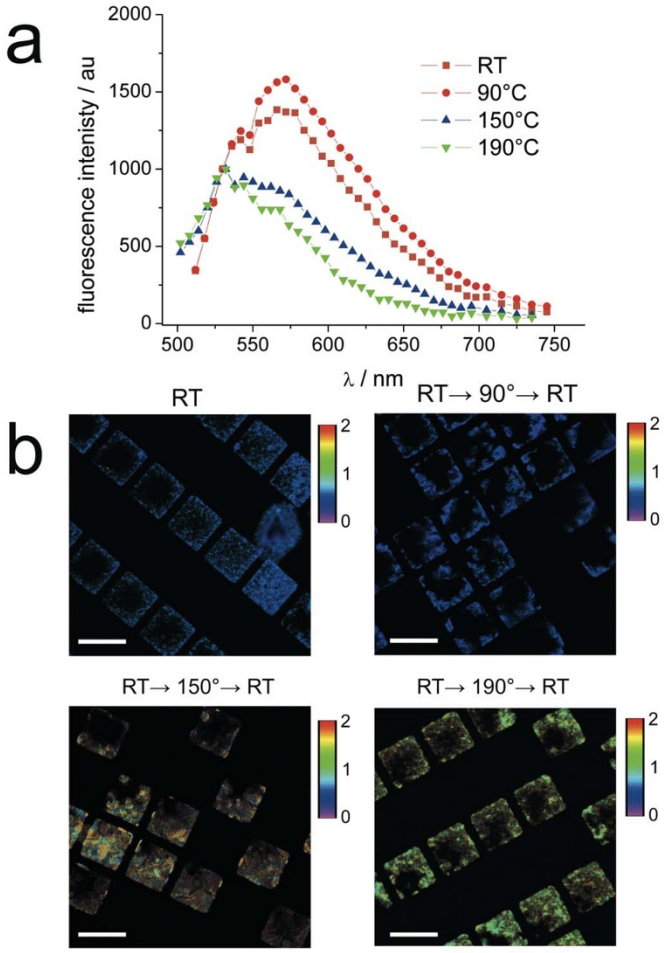

Figure 5 | Laser scanning confocal fluorescence microscopy characterization of polycrystalline thin films. (a) Evolution of the confocal photoluminescence spectrum upon thermal treatment. (b) Confocal images in ratio view (I_{520}/I_{585}) of the fluorescence intensity measured contemporarily with two PMTs cantered at 520 and 585 nm. The same behaviour was observed both in thin film and patterned samples.

Time temperature integrator. Cast films were very stable and no effects of aging were observed even after keeping the sample in ambient conditions for few months. Accordingly, the Differential Scanning Calorimetry (DSC) (see supplementary information) thermogram does not show peaks before 200°C (at 200°C **1** exhibits a phase transition corresponding to the crystal → liquid crystal).

While the thin deposit of large crystals (prepared by drop casting from toluene solution) remained almost unaltered up to 200°C, the polycrystalline films (prepared by drop casting in air from chloroform solution) exhibited an irreversible structural change accompanied by changes in the photoluminescent properties. The confocal PL spectra (Fig. 5a) shift from yellow to green upon thermal treatment. This is clearly evidenced by the confocal images in figure 5b reporting a ratio view of the green and orange PL intensity in polycrystalline thin film. The ratio (I_{520}/I_{585}) increases from 0.5 ca. in the film at room temperature up to 2.0 in the films exposed at 190°C. This tendency is confirmed by the evolution of fluorescence lifetime, which shows that the lifetime of 1.3 ± 0.2 ns dominates at room temperature, while the lifetime of 0.45 ± 0.1 ns becomes progressively the dominant one for samples exposed at higher temperatures. Likely, this behaviour is due to the transition of microcrystals from the phase of fibers to the more stable phase corresponding to platelets.

These results prompted us to develop a TTI able to integrate monolithically, viz. in a single material, the capability to monitor and record different temperatures.

In order to have a reference colour and to perform a quantitative reading of the device, the TTI was fabricated by patterning a data matrix made of micrometric structures of **1** on silicon substrates. This configuration allowed us to combine the TTI functionality with the information storage capability. In particular we fabricated a logic pattern containing information in a binary code formed by micrometer-size pixels detectable by a conventional optical microscope. The targeted pattern had a regular distribution of holes with 18 × 18 μm² lateral size and 1 μm depth (pixels) on a substrate of SiO_2 (Fig. 6b).

Thin deposits were obtained by drop casting a solution of **1** on the patterned substrate (20 μl/cm²). As the solvent shrank and its volume became comparable with the volume of the pixels, due to the higher surface tension the solution remained preferentially pinned in correspondence of the pixels. When the solution reached

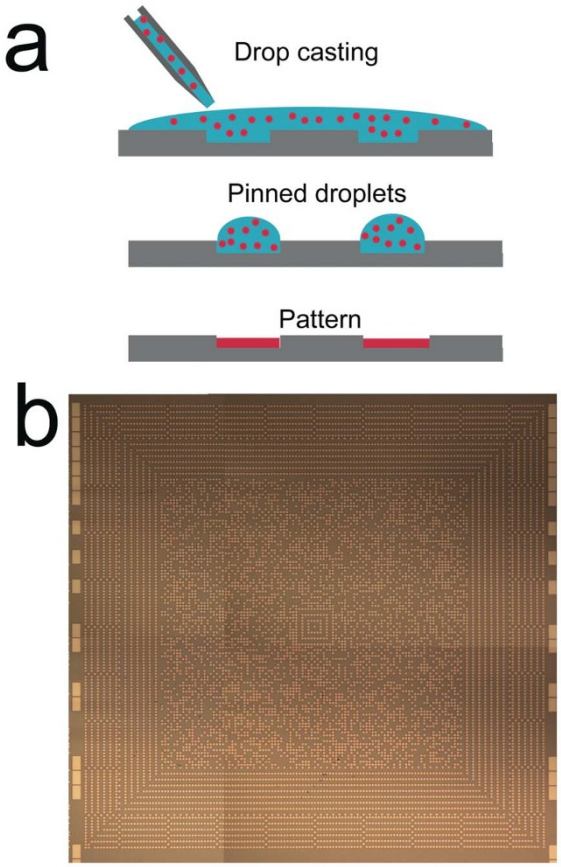

Figure 6 | Patterning. (a) Scheme of the process. (b) Optical micrograph of pattern of holes representing a data matrix. The total size of the image is 3×3 mm^2; each pixel is $18 \times 18 \times 1$ μm^3.

the supersaturation it precipitated into the pixels, forming a perfectly regular pattern (see cartoon in fig. 6a and fig. 7). Using a solution with a concentration 2 g/L $<$ C $<$ 4 g/L all pixels were completely filled by **1**. Using a lower concentration the material was

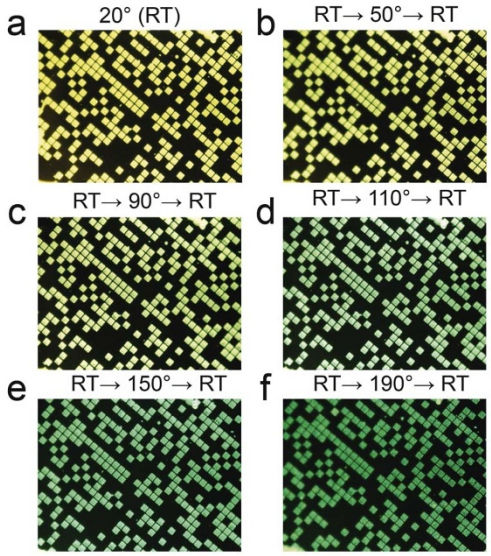

Figure 7 | Evolution of the fluorescence in patterned film recorded by a CCD versus the temperature. The images were taken at room temperature, using a band pass filter $>$ 475 nm, after heating the pattern at the indicated temperature for 30 seconds (no further changes were observed after this time).

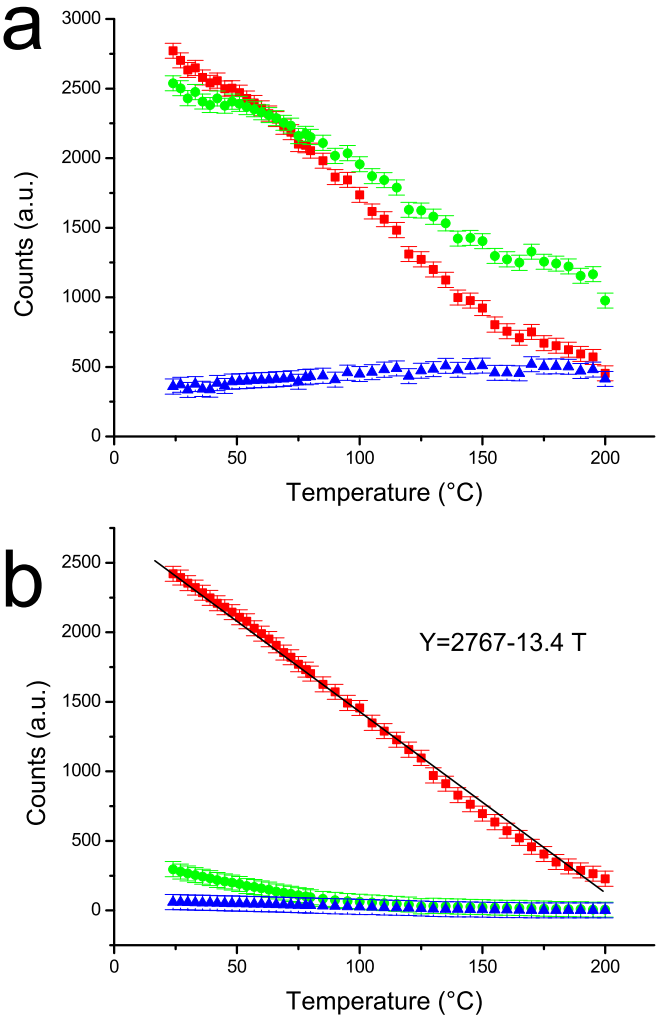

Figure 8 | Quantitative analysis of the fluorescence images. A commercial CCD recorded fluorescence images. The colours of the graphs correspond to the colours component of the CCD (red, blue, green). (a) Number of counts versus temperature obtained using a filter Ex 420, DM 435, BA 475, which enables the transmission of all visible components except a slight portion of the blue. (b) Number of counts versus temperature obtained using a filter Ex 535, DM 570, BA 590, which transmits only the red component. Each image was recorded fixing the intensity of illumination and the time of acquisition of the CCD.

inhomogeneously distributed inside the pixel and accumulated at the pixel corners (see also the image of ToC). Figure 7 shows an image of the pattern employed in our experiments. Patterned samples have the same characteristics of the thin deposit prepared by drop casting from chloroform solution in air, i.e. they are formed by polycrystals and appear yellow upon FM (Fig. 7a). Heating the sample we observed a progressive change of the fluorescence images from yellow to green in the temperature range 20–200°C. Figure 7a–f shows the colour evolution with the temperature measured by FM. Noticeably, if the pattern is heated at the indicated temperature for more than 30 s, this change becomes irreversible.

A commercial CCD recorded fluorescence images during the thermal treatment using two filters for fluorescence. Figure 8 show the number of counts (NCs) of the red, green and blue component recorded by the CCD as a function of the temperature at which the device was exposed for 30 s. Note that the optical filters used allow the transmission of all visible components but cuts a slight portion of the blue (Fig. 8a) and the red component (Fig. 8b); each image was

recorded fixing the intensity of illumination and the time of acquisition of the CCD (see detail in the method section).

Discussion

The quantitative analysis of the fluorescence images (Fig. 8) clearly shows that for each temperature the colour recorded by the CCD is formed by a unique and defined combination of Red, Green and Blue (RGB) components and that the red component undergoes the most pronounced variation with temperature. Figure 8b shows the NCs RGB components recorded by the CCD using an optical filter, which allows the transmission of the red component only. As clearly shown by the graph we observed a linear decrease of the red component with the temperature. Therefore, the temperature at which the device was exposed can be analytically derived from the NCs of the red fluorescence image according to the linear fit NC = 2767 -13.4 T with an error of about ± 2 C. Noticeably, heating the sample at different temperatures (we tested our devices upon many tens of cycles), patterned films are stable and record the highest temperature of which it was exposed for more than 30 s. Eventually, in order to demonstrate the effective reversibility/irreversibility of the system, we verified the effect of cooling down to 270 K, which is the relevant range of temperatures for many applications in food and pharm industries. We verified that the samples always preserve the properties originated by the highest exposure temperature, provided that the exposure lasts more than 30 s.

In summary, we presented a new application of fluorescent oligothiophene thin films where the exposure to a specific temperature tailors the fluorescence emission. In particular we advantageously exploited two phenomena that are usually drawbacks for technological applications, such as polymorphism and recrystallization. These properties allow us to fabricate patterns with time temperature integration functionalities in an impressive range of temperatures (i.e. from room temperature to 200°C) by using a single active material.

We demonstrated the feasibility of the approach by a simple fabrication method, using **1** as a model compound, however, this approach is general and can be extended to all functional materials, whose fluorescence, or colour, or other photophysical properties, change irreversibly with temperature.

The easy processing and the use of a single material, combined with the possibility of interrogating the device by a simple optical technique, make our approach extremely appealing for the development of a new generation of low-cost TTIs working in a wide range of temperatures.

Methods

Thin deposits. Thin deposits of **1** were prepared by drop casting of 20 μl/cm^2 of a 1 g/L solution in toluene or chloroform on Si/SiO_2 wafers. The solvent was slowly evaporated at room temperature in a solvent-saturated atmosphere or in air. The substrates consist of a 10 × 10 mm^2 piece of silicon covered by 200 nm of thermal oxides or pre-paterned Si/SiO_2 substrates fabricated by photolithography. It was cleaned by: sonication for 2 min. in electronic-grade water (milli-pure quality), 2 min. in acetone then 2 min. in 2-propanol.

Optical microscopy. Optical micrographs were recorded with a Nikon i-80 microscope equipped with epi-illuminator and cross polars (POM). All the images presented were recorded using objective: LU Plan ELWD 20X/0.40 objective.

Fluorescence microscopy. Fluorescence images were recorded with a Nikon i-80 microscope equipped with epi-fluorescence (FM) using FM filter Nikon Ex 420, DM 435, BA 475 and Ex 535, DM 570, BA 590. The FM images were recorded using a commercial CCD camera (Nikon Nikon CCD DS-2 Mv). The illumination was performed by a 100 W halogen lamp at fixed power (i.e. tension 12 V) and with fixed time of acquisition of the CCD (500 ms). Images colour composition were analysed by software Graphic Converter X.

Thermal annealing. The thermal annealing were performed under the optical microscope using a heating stage Linkham TMHS600 connected to a TP94 controller, with a control of 0.1°C using the setup described in ref. 32.

X-ray diffraction analysis was carried out by means of a PANalytical X'Pert diffractometer equipped with a copper anode (λ_{mean} = 0.15418 nm) and a fast X'Celerator detector. Step 0.05° (2theta scale), counting time 400 sec.

Laser Scanning Confocal Fluorescence imaging was performed on an inverted Nikon A1 laser scanning confocal microscope equipped with a 405 nm pulsed/CW diode laser (Picoquant, Germany) and a 488 nm CW Argon ion laser (Melles Griot). Confocal fluorescence imaging was carried out on the samples at RT. The 521 × 512 or 1024 × 1024 pixel images were collected using a Nikon PLAN APO VC 60 oil immersion objective with NA 1.40. With this imaging configuration, pixel side dimension ranged from 100 to 250 nm. Hexagonal pinhole dimension was set to 0.8 au corresponding to 25 mm and optical thickness of 330 nm. A dichroic mirror reflecting 405, 488, 541 and 640 was used. Fluorescence was collected in several spectral windows. In front of the photomultiplier we used bandpass filters centered at 525 nm (50), 595 (50) and 700 nm (75). *Spectral imaging* has been performed using the Nikon A1 spectral detector consisting of a multi-anode photomultiplier with an array of 32 anodes. A wavelength range of 6 or 10 nm per anode has been applied. For fluorescence lifetime imaging a time-correlated single photon counting (TCSPC) system of Picoquant GmbH Berlin was used exciting at 405 nm. Photons were detected in TTTR mode with a Single Photon Avalanche Diode (SPAD) manufactured by Micro Photon Devices (MPD), Bolzano, Italy. Fluorescence was filtered with the opportune fluorescence SEMROCK bandpass filters 585/40 nm, and 520/40 nm. PicoHarp 300 photon processor completes the TCSPC system. SymPhoTime v. 5.1 analysis software was used for image processing and lifetime fitting. A tail fit with multi-exponential functions was performed to analyze fluorescence decays of selected ROI. The system allowed measurement of fluorescence lifetimes from 300 ps up to several nanoseconds.

Atomic force microscopy. AFM images were recorded with a commercial AFM (MultiMode 8, Bruker) operating in tapping or peak-force mode in ambient condition. Image analysis was done using the open source SPM software Gwyddion-www.gwyddion.net.

1. Dimitrakopoulos, C. D. & Malenfant, P. R. L. Organic thin film transistors for large area electronics. *Adv. Mater.* **14**, 99 (2002).
2. Greco, P. *et al.* Conductive sub-micrometric wires of platinum-carbonyl clusters fabricated by soft-lithography. *J. Am. Chem. Soc.* **130**, 1177–1182 (2008).
3. Serban, D. A. *et al.* Towards all-organic field-effect transistors by additive soft lithography. *Small* **5**, 1117–1122 (2009).
4. Melucci, M. *et al.* Thienopyrrolyl dione end-capped oligothiophene ambipolar semiconductors for thin film- and light emitting transistors. *Chem. Commun.* **47**, 11840–11842 (2011).
5. Muccini, M. A bright future for organic field-effect transistors. *Nat. Mater.* **5**, 605–613 (2006).
6. Lambert, A. G., Davies, P. B. & Neivandt, D. J. Implementing the theory of sum frequency generation vibrational spectroscopy: A tutorial review. *Appl. Spectrosc. Rev.* **40**, 103–145 (2005).
7. Sirringhaus, H., Tessler, N. & Friend, R. H. Integrated optoelectronic devices based on conjugated polymers. *Science* **280**, 1741–1744 (1998).
8. Kim, Y. *et al.* A strong regioregularity effect in self-organizing conjugated polymer films and high-efficiency polythiophene: fullerene solar cells. *Nat. Mater.* **5**, 197–203 (2006).
9. Taliani, C. *et al.* Organic-inorganic hybrid spin-valve: A novel approach to spintronics. *Phase Transitions* **75**, 1049–1058 (2002).
10. Cavallini, M., Facchini, M., Albonetti, C. & Biscarini, F. Single molecule magnets: from thin films to nano-patterns. *Phys. Chem. Chem. Phys.* **10**, 784–793 (2008).
11. Cavallini, M. *et al.* Thin Deposits and Patterning of Room-Temperature-Switchable One-Dimensional Spin-Crossover Compounds. *Langmuir* **27**, 4076–4081 (2011).
12. Murray, K. S. & Kepert, C. J. Cooperativity in spin crossover systems: Memory, magnetism and microporosity. *Spin Crossover in Transition Metal Compounds I* **233**, 195–228 (2004).
13. Melucci, M. *et al.* Multicolor, large-area fluorescence sensing through oligothiophene-self-assembled monolayers. *Chem. Commun.* **47**, 1689–1691 (2011).
14. Cavallini, M., Facchini, M., Massi, M. & Biscarini, F. Bottom-up nanofabrication of materials for organic electronics. *Synth. Met.* **146**, 283–286 (2004).
15. Cavallini, M. Inhomogeneous thin deposits: a strategy to exploit their functionality. *J. Mater. Chem.* **19**, 6085–6092 (2009).
16. Mishra, A., Ma, C.-Q. & Bäuerle, P. Functional Oligothiophenes: Molecular Design for Multidimensional Nanoarchitectures and Their Applications. *Chem. Rev.* **109**, 1141–1276 (2009).
17. Roncali, J. Molecular Bulk Heterojunctions: An Emerging Approach to Organic Solar Cells. *Acc. Chem. Res.* **42**, 1719–1730 (2009).
18. Barbarella, G., Melucci, M. & Sotgiu, G. The Versatile Thiophene: An Overview of Recent Research on Thiophene-Based Materials. *Adv. Mater.* **17**, 1581–1593 (2005).
19. Surin, M. *et al.* Solid-state assemblies and optical properties of conjugated oligomers combining fluorene and thiophene units. *J. Mater. Chem.* **17**, 728–735 (2007).

20. Leclere, P. *et al.* Surface-controlled self-assembly of chiral sexithiophenes. *J. Mater. Chem.* **14**, 1959–1963 (2004).
21. Cavallini, M., Gentili, D., Greco, P., Valle, F. & Biscarini, F. Micro- and nanopatterning by lithographically controlled wetting. *Nat. Protoc.* **7**, 1668–1676 (2012).
22. Cavallini, M. *et al.* Ambipolar multi-stripe organic field effect transistors. *Adv. Mater.* **23**, 5091–5097 (2011).
23. Facchetti, A. Semiconductors for organic transistors. *Materials Today* **10**, 28–37 (2007).
24. Melucci, M. *et al.* Thiophene-Benzothiadiazole Co-Oligomers: Synthesis, Optoelectronic Properties, Electrical Characterization, and Thin-Film Patterning. *Adv. Funct. Mater.* **20**, 445–452 (2010).
25. Cavallini, M. *et al.* Field-effect transistors based on self-organized molecular nanostripes. *Nano Lett.* **5**, 2422–2425 (2005).
26. Lu, J. P., Xia, P. F., Lo, P. K., Tao, Y. & Wong, M. S. Synthesis and properties of multi-triarylamine-substituted carbazole-based dendrimers with an oligothiophene core for potential applications in organic solar cells and light-emitting diodes. *Chem. Mater.* **18**, 6194–6203 (2006).
27. Manske, W. J. Selected time interval indicating device. *US Patents 3,954,011,1976* (1976).
28. Taoukis, P. S. & Labuza, T. P. *J. Food Sci.* **54**, 783–788 (1989).
29. Cavallini, M. *et al.* Lithographic Alignment of Discotic Liquid Crystals: A New Time-Temperature Integrating Framework. *Adv. Mater.* **21**, 4688–4691 (2009).
30. Calo, A., Stoliar, P., Matacotta, F. C., Cavallini, M. & Biscarini, F. Time-Temperature Integrator Based on the Dewetting of Polyisobutylene Thin Films. *Langmuir* **26**, 5312–5315 (2010).
31. Durso, M. *et al.* Synthesis, size-dependent optoelectronic and charge transport properties of thie-no(bis)imide end-substituted molecular semiconductors. *Org. Electron.* (2013), DOI: http://dx.doi.org/10.1016/j.orgel.2013.07.019.
32. Calo, A., Stoliar, P., Cavallini, M., Geerts, Y. H. & Biscarini, F. Synchronized optical and electrical characterization of discotic liquid crystals thin films. *Rev. Sci. Instrum.* **81**, 033907 (2010).

Author contributions

D.G. was responsible for all the experiments described in this article; M.D., C.B. synthetized the material, M.G. performed X-Ray measurements, I.M. performed LSCM measurements R. C., Mi.Mu., R.C. were partially responsible for preparation of the paper; M.C. and Ma.Me. were responsible for designing and providing guidance for the experiments and for editing and proofreading the paper. All the authors contributed to write the manuscript.

Additional information

Supplementary information accompanies this paper at http://www.nature.com/scientificreports

Competing financial interests: The authors declare no competing financial interests.

How to cite this article: Gentili, D. *et al.* A time-temperature integrator based on fluorescent and polymorphic compounds. *Sci. Rep.* **3**, 2581; DOI:10.1038/srep02581 (2013).